Optics Letters

Pose-varied swing arm profilometer test for off-axis aspheric surfaces with strong asphericity

LING XIONG,* XIAO LUO, XUEJUN ZHANG, ERHUI QI, HAIXIANG HU, ZHENYU LIU, AND FENG ZHANG

Key Laboratory of Optical System Advanced Manufacturing Technology, Changchun Institute of Optics, Fine Mechanics and Physics, Chinese Academy of Sciences, Changchun 130033, China

**Corresponding author: xiongling@ciomp.ac.cn*

Received 13 July 2021; revised 14 August 2021; accepted 19 August 2021; posted 7 September 2021 (Doc. ID 435200); published 29 September 2021

The swing arm profilometer (SAP) has been widely used to test large aspheric optics by measuring the asphericity from its best-fitting sphere (BFS). To further improve the test accuracy, we propose a pose-varied test mode for the SAP with a shorter-range probe to measure off-axis aspheric surfaces with stronger asphericity. In contrast to the classical SAP mode in which the air-table is fixed in a stationary position during measurement, we adjust the pose of each scan arc to match the local BFS and the measurement range of the probe decreases to half that of the global asphericity. To verify the effectiveness, we conduct experiments on an off-axis asphere with a diameter of 3 and 2 m. Compared with a classical SAP mode, it achieved an improved performance of 50% higher repeatability and 32% higher accuracy.

https://doi.org/10.1364/OL.435200

The swing arm profilometer (SAP) test was originally proposed by Anderson *et al*. from the University of Arizona [1]. They built a profilometer based on the geometry of a sphere generator. It was first used to achieve highly accurate and efficient measurements for convex aspheric optics. The test accuracy was approximately 1 micron with a single arc detected [1,2]. Over recent years, numerous studies on improving the testing accuracy of SAPs have been conducted. The Arizona group applied self-calibration on an air-table using a dual-probe shear test; they realized a root mean square (RMS)-based calibration accuracy of 3 nm for a convex test sample with a diameter of 350 mm. They also reported on the calibration of a sensor for measuring an aspheric ground surface with a diameter of 1 m and reported an RMS-based accuracy of approximately 100 nm [3,4]. Numerous other studies have been conducted on the calibration of SAP parameters, such as the measurement of arm length and the error separation of air-bearing. In these studies, the RMS-based test uncertainty of the SAP setup was reported to be approximately 0.5 um [5–7].

In our laboratory, we used an SAP to test optics with a large diameter and guide surface grounding prior to the polishing process. Because a higher-accuracy SAP test for mirrors, especially those composed of silicon carbide (SiC), will observably help improve fabrication efficiency [8], the study in this Letter aimed to achieve the highest possible accuracy of SAPs. Therefore, we propose a hanging SAP with a short arm to achieve an RMS-based test accuracy of 0.1 um by conducting tests on an aspheric mirror with a diameter of 2 m. We also conducted tests using a stitching SAP to maintain high test accuracy for larger optics [9,10]. Moreover, we demonstrated calibrations, such as probe correction and air-bearing calibration. In a classical SAP mode, the measurement range of the indicator should be larger than the asphericity of the global best-fitting sphere (BFS). For larger aspheric optics, the test accuracy decreased as the measurement range increased. This aspect is a limitation for improving test accuracy. It would be optimal if the aspheric surface with a higher departure could be measured using a probe with a shorter range.

In this Letter, we devise a concept for achieving this goal. We propose an approach for generating a pose-varied SAP (pvSAP) test and minimize the measurement range of scan arcs to half that of the asphericity.

First, we introduce the classical pose-fixed SAP (pfSAP) test principle. Secondly, we conduct a simulated SAP test and calculate the tilt and piston value in each scan arc. Considering the degrees of freedom of the SAP setup, we determine the pose of the SAP setup for each scan arc to compensate for the tilt and piston. Using the above, we build a pvSAP test model, and the required probe measurement range decreases compared to the pfSAP test. Lastly, we implement a pvSAP test on an off-axis aspheric mirror with a diameter of 3 m to verify enhanced test accuracy.

The principle of the classical pfSAP test is presented in Fig. 1(a). A probe was mounted at the end of an arm, which was fixed on a high-accuracy air-table; the rotating axis of the air-table was tilted and passed through the center of the BFS of the asphere under test [9]. The aspheric mirror was placed on a worktable. During measurement, the air-table was fixed in a stationary position, and the probe was rotated about the axis of the air-table to complete arc scanning. After the arc was scanned, the worktable was rotated by an angle α. The probe then swung across the mirror to complete the next arc scanning. By rotating the worktable, multiple scans were obtained showing a three-dimensional profile, as presented in Fig. 1(b), where the first arc

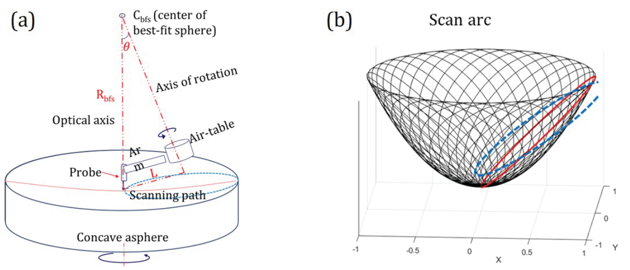

Fig. 1. (a) Schematic diagram of the SAP test. (b) Profiling pattern of scan arcs.

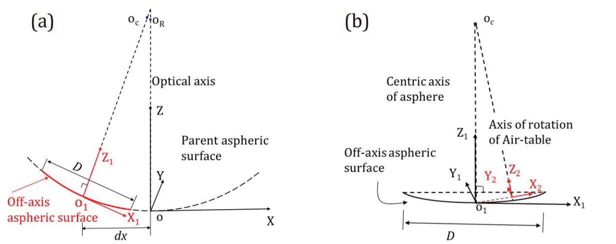

Fig. 2. (a) Relative position of the off-axis surface. (b) BFS from the off-axis surface in a coordination system of the SAP.

is marked in red. The tilt-angle θ of the air-table and the rotated angle α of the worktable are expressed as follows:

$$\theta{=}\sin^{-1}\left(L\big/ R_{\mathrm{bfs}}\right), \tag{1}$$

$$\alpha{=}2\pi\big/ N, \tag{2}$$

where L represents the distance between the probe tip and the rotation axis of the air-table, and R_{bfs} represents the radius of curvature of the BFS. N represents the number of scan arcs.

The position of an off-axis aspheric surface in the coordination system of the parent mirror is shown in Fig. 2(a). The asphericity differs according to different definitions. Considering the rotational symmetry of the SAP test, the center point O_c of the BFS of the aspheric surface is set on the geometric centric axis of the mirror [9], as shown in Fig. 2(b). The asphericity mentioned in this Letter is defined as the minimum departure from the BFS in the peak-to-valley (PV), and the coordinate system of the SAP test is the (O_1, X_1, Y_1, Z_1) coordinate system as displayed below.

The asphericity of an off-axis parabolic mirror with a diameter of 3 m and an off-axis displacement of 2000 mm is approximately 1300 µm in the PV, as shown in Fig. 3(a). The arc marked in red indicates the relative pose of the first arc from the perspective of the sphere base and its asphericity mainly consisting of tilt. We considered that the pose of the red arc could be adjusted to remove the tilt and fit the local asphericity, as the blue arc displayed. Thus, the measured asphericity would decrease significantly. Figure 3(b) shows the simulated probe readout of the arc. The red curve corresponds to the readout of the first arc in the classical pfSAP mode. The blue dashed curve represents the readout of the first arc with the tilt removed, corresponding to the local asphericity. Based on this, we can vary the pose of the scan arc to remove the local tilt and retrench the measurement range. This allowed for the use of a probe with a shorter range, as well as higher precision. Therefore, a higher accuracy of measurement could be achieved.

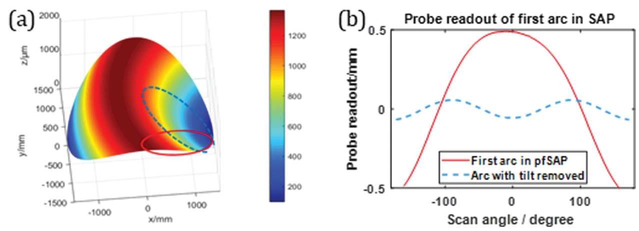

Fig. 3. (a) Departure from the BFS of an aspheric surface with a diameter of 3 m. (b) Probe readout of the first arc.

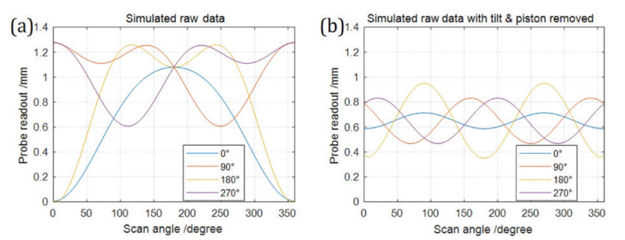

Fig. 4. Simulative profile test of a perfect off-axis mirror with work-table rotated by 0°, 90°, 180°, and 270°. (a) Probe readouts of the scan arcs and (b) probe readouts with the tilt and piston removed.

A classical pfSAP test for the off-axis mirror with a diameter of 3 m was simulated when work-table was rotated by 0°, 90°, 180°, and 270° separately. The probe readout of typical arcs was presented in Fig. 4(a); the range of readouts was within 1.3 m. The values of the tilt and piston from the probe readouts can be extracted using Eq. (3), as follows:

$$S = a\cdot L\cdot\cos(\beta) + b\cdot L\cdot\sin(\beta) + c, \tag{3}$$

where S represents the probe readout, L represents the scan radius of the arc, β represents the scan angle of the arc, a and b represent the fit coefficients of tilt about the axes Y_2 and X_2, and c represents the piston fitted along the axis Z_2. Axes X_2, Y_2, and Z_2 are presented in Fig. 2(b). The probe readout after the local tilt and the piston are removed is presented in Fig. 4(b), where the range of the probe readout is reduced to half that of the asphericity.

For the pvSAP test, the tilt and piston from each scan arc in the pfSAP mode were removed by the varying poses of the air-table. During a measurement, the SAP setup was mounted on the gantry numerical control machine tool (GNCMT) to allow *in situ* measurements. The degrees of freedom of the SAP setup are the tilt around the Y_1 axis and movement along the X_1, Y_1, and Z_1 axes of the coordinate system (O_1, X_1, Y_1, Z_1) shown in Fig. 2(b). For an aspheric surface test, compensation for the free tilt of the air-table around X_1 can be achieved by moving the piston along Y_1 instead [9]. Hence, the pose compensation for of the air-table for the scan arcs can be extracted as follows:

$$S = \tan(Tilt_X)\cdot L\cdot\cos(\beta) + \tan(Tilt_Y)\cdot L\cdot\sin(\beta) + Pist_Z, \tag{4}$$

$$Pist_Y = R_{\mathrm{bfs}}\cdot\tan(Tilt_Y), \tag{5}$$

where $Tilt_X$ and $Tilt_Y$ represent the tilt angle of the air-table around the Y_1 and X_1 axes, respectively, and $Pist_Y$ and $Pist_Z$ represent displacements along the Y_1 and Z_1 axes, respectively.

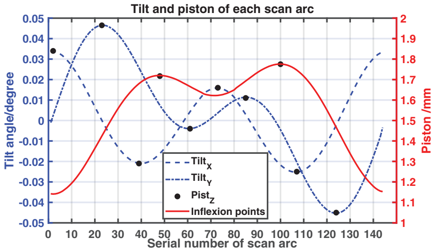

Fig. 5. Simulated tilt and piston of 144 scan arcs for the aspheric surface with a diameter of 3 m.

Table 1. Parameters of the Typical Inflection Points Marked on the Pose Curve Shown in Fig. 5

Serial Number of Scan Arc	Tilt around Axis Y_1 (°)	Tilt around Axis X_1 (°)	Piston Alone Axis Y_1/mm	Piston Alone Axis Z_2/mm
2	0.034	0.002	0.604	1.141
23	0.000	0.047	12.021	1.424
39	−0.021	0.026	6.641	1.680
48	−0.016	0.007	1.925	1.720
61	0.004	−0.004	−1.022	1.666
73	0.016	0.004	0.963	1.623
85	0.003	0.011	2.944	1.693
100	−0.022	−0.005	−1.173	1.776
107	−0.025	−0.020	−5.251	1.746
124	−0.002	−0.045	−11.701	

To analyze the characteristics of the varied pose, the tilt angle and piston of 144 scan arcs were simulated, and the results are shown in Fig. 5. Ten inflexion points on the curves were marked, and the corresponding poses of arcs are presented in Table 1. The tilt angle of the air-table around the Y_1 axis ranged from $--0.025°$ to $+0.034°$. The tilt around the X_1 axis ranged from $-0.045°$ to $0.047°$, where the equivalent piston displacement along Y_1 ranged from −11.701 to 12.021 mm. The piston displacement along Z_1 ranged from 1.141 to 1.776 mm to the best fit into the center range of the probe readout.

It is time-consuming and inefficient to check the compensated poses of all scan arcs before testing. Hence, only the practical compensated poses of the tilts and displacements were checked. The typical pose values of the arcs are given in Table 1. The approach for checking the compensated poses of the arcs before testing was presented as follows:

(1) The tilt and piston of each scan arc from the classical pfSAP test were simulated. Ten typical inflection points on the pose curves were selected, as shown in the points marked on the curves in Fig. 5.
(2) The corresponding tilt and piston for the 10 arcs were checked by moving and rotating the air-table to minimize the local tilt value. The data are shown in Table 1.
(3) The tilt and piston of the rest of the arcs to be compensated for were generated from the pose curve whose value of inflexion points were amended from the practical pose data presented in step 2.
(4) The pvSAP test was started. The air-table was adjusted to the first position with the pose compensated for; the first arc was scanned. After the first arc was scanned, the air-table was auto-adjusted to the next position and remained stationary until the scanning of the second arc was completed. The same process was followed for the next arc scans.

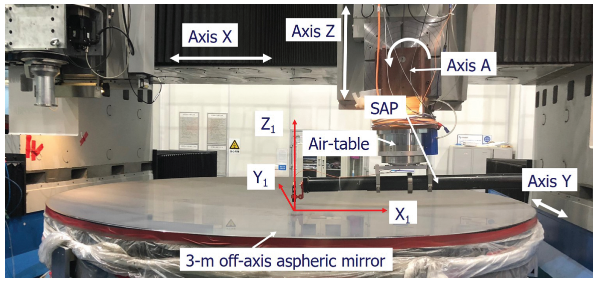

Fig. 6. SAP setup for an off-axis aspheric mirror with a diameter of 3 m.

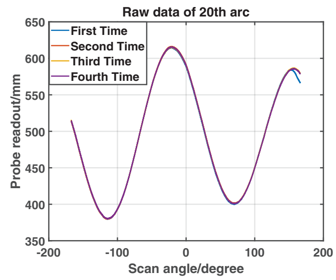

Fig. 7. Raw data of the 20th arc repeatedly scanned four times.

To verify the effectiveness of the pvSAP mode, we implemented the classical pf SAP test and pvSAP test on the SiC off-axis aspheric mirror with a diameter of 3 m. The SAP setup was demonstrated in Fig. 6, where the coordinate system (O_1, X_1, Y_1, Z_1) and freedom of degrees were displayed. We used a Micro-Epsilon optical probe (IFS 2401-3) with a measurement range of 3 mm, linearity of 1.5 μm, and resolution of 0.12 μm. The initial tilt angle θ of the air-table was 2.946°. The length of the arm L was 760.54 mm.

The position data of the air-table for each arc were imported into the GNCMT machine, and an auto test was started. The air-table arrived at the first position, and the probe scanned back and forth twice. Next, the air-table arrived at the second position, and the work table rotated by 2.5°. The probe scanned back and forth twice again as did the rest of the arcs. Therefore, 144 arcs were repeatedly scanned four times.

Compared to the classical pfSAP test during which the air-table was fixed on just one pose, each arc in the pvSAP mode was posture-adjusted before scanning, and kinematic effects may exist at the beginning of the scanning process. As shown in Fig. 7, the arc was scanned from $+180°$ to $--180°$ and then back and forth twice; four sets of repeatedly scanned data were obtained. There was a little instability during the beginning of the first scan time.

To avoid disturbances from the kinematic effect, data from first scan time of each arc were abandoned, data from the last three times were averaged to reduce the effect of random noise, and averaged value was used to resolve the surface map. Figure 8(a) shows the averaged raw data from the classical pfSAP test, and Fig. 8(b) shows the averaged raw data of the pvSAP test. The range of the probe reading was decreases from 1.8 to

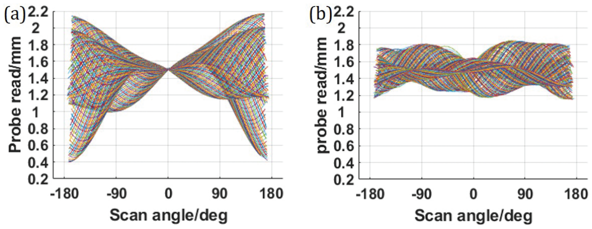

Fig. 8. Scan data of 3 m mirror tested by the (a) pfSAP mode and (b) pvSAP mode.

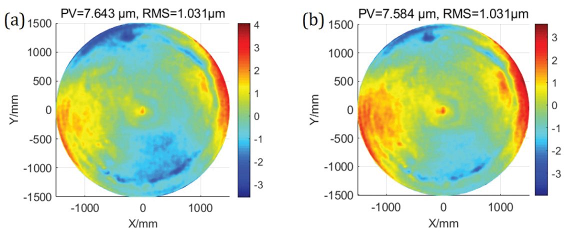

Fig. 9. pvSAP test results for an off-axis aspheric surface with a diameter of 3 m.

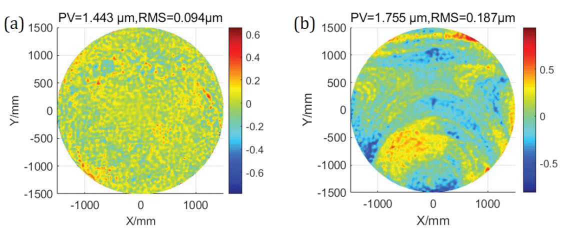

Fig. 10. Measurement repeatability of 3 m mirror tested using the (a)_pvSAP mode and (b) classical pfSAP mode with the piston, tilt, power, and astigmatism removed.

1.0 mm. It was slightly larger than the simulated value of the asphericity owing to residuals from assembly.

Two surface maps tested by the pvSAP mode are shown in Fig. 9. The map results were 7.643 and 7.584 μm in the PV separately, and 1.031 μm in RMS. Their test repeatability was 1.443 μm in the PV and 0.094 μm in RMS, as shown in Fig. 10(a). The test repeatability of the classical pfSAP test mode with astigmatism removed was 1.755 μm in the PV and 0.187 μm in RMS, as shown in Fig. 10(b). Compared to the classical mode, the pvSAP mode exhibited an improved performance with a higher repeatability of 50%.

Furthermore, to verify the accuracy improvement of pvSAP mode, we conducted an accurate test comparison for a ø2 m off-axis aspheric mirror (as a standard component), whose asphericity in full aperture was a 1.1 mm PV and surface error was $\lambda/40$ RMS ($\lambda = 633$ nm, CGH test results) measured by the ZYGO Interferometer, as shown in Fig. 11.

The surface map was 1.164 μm in the PV and 0.179 μm in RMS tested in the classical pfSAP mode and 0.988 μm in the PV and 0.121 μm in RMS tested in the pvSAP mode. Compared with a classical pfSAP test, measurement accuracy of the pvSAP was improved by 32% in RMS.

In this Letter, we propose a method to reduce the measurement range to half that of the asphericity by testing the

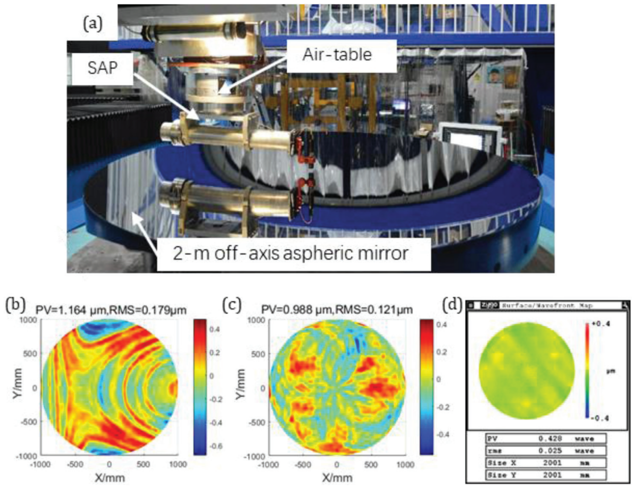

Fig. 11. (a) SAP setup for testing a ø2 m standard off-axis aspherical mirror. (b) Test results from the pfSAP mode, (c) test results from the pvSAP mode, and (d) surface map measured by a ZYGO Interferometer with the piston, tilt, power, astigmatism, coma, and trefoil removed.

local aspheric departure in each arc. Compared to the classical pfSAP test, the measurement range of the required probe decreased by 50% directly, and test repeatability was improved by 50% accordingly. The test accuracy was promoted by 32%. Alignment before the pvSAP test in the study in this Letter was based on the pfSAP with a long-range displacement sensor. Depending on the sensor readout, the poses of 10 typical scan arcs were adjusted and checked. For general application, there will be no long-range probes for assistance. Further works will focus on how to adjust the pose with a shorter-range probe, and the pvSAP mode would be used directly to achieve the higher test accuracy.

Funding. Chinese Academy of Sciences Key Project; National Natural Science Foundation of China (61805243, 62005278).

Disclosures. The authors declare no conflicts of interest.

Data Availability. No data were generated or analyzed in the presented research.

REFERENCES

1. D. S. Anderson, R. E. Parks, and T. Shao, in *Proceedings of OF&T Workshop Technical Digest* (1990), Vol. **11**, p. 119.
2. D. S. Anderson and J. H. Burge, Proc. SPIE **2536**, 169 (1995).
3. P. Su, Y. Wang, J. O. Chang, R. E. Parks, and J. H. Burge, Proc. SPIE **8126**, 50 (2011).
4. Y. Wang, P. Su, R. E. Parks, J. O. Chang, and J. H. Burge, Opt. Eng. **51**, 073606 (2012).
5. H. Jing, C. King, and D. Walker, Opt. Express **18**, 2036 (2010).
6. H. Jing, C. King, and D. Walker, Proc. SPIE **7656**, 765662 (2010).
7. H. Jing, C. Lin, L. Kuang, S. Wu, F. Wu, and T. Fan, Proc. SPIE **8415**, 84150K (2012).
8. X. Luo, Chin. Opt. Lett. **12**, S22202 (2014).
9. L. Xiong, X. Luo, Z. Liu, X. Wang, H. Hu, F. Zhang, L. Zheng, and X. Zhang, Opt. Eng. **55**, 074108 (2016).
10. L. Xiong, E. Qi, X. Luo, F. Zhang, D. Xue, and X. Zhang, Chin. Opt. Lett. **17**, 112201 (2019).